

MoS₂/h-BN heterostructures: controlling MoS₂ crystal morphology by chemical vapor deposition

Aspasia Antonelou^{1,2}, T. Hoffman³, J. H. Edgar³, and Spyros N. Yannopoulos^{1,*}

Received: 29 November 2016 Accepted: 17 February 2017 Published online: 15 March 2017

© Springer Science+Business Media New York 2017

ABSTRACT

Tuning the properties of van der Waals heterostructures based on alternating layers of two-dimensional materials is an emerging field of research with implications for electronics and photonics. Hexagonal boron nitride (h-BN) is an attractive insulating substrate for two-dimensional materials as it may exert less influence on the layer's properties than silica. In this work, MoS₂ layers were deposited by chemical vapor deposition (CVD) on thick h-BN flakes mechanically exfoliated deposited on Si/SiO₂ substrates. CVD affords the controllable, large-scale preparation of MoS₂ on h-BN alleviating shortcomings of manual mechanical assembly of such heterostructures. Electron microscopy revealed that in-plane and vertical to the substrate MoS₂ layers were grown at high yield, depending on the sample preparation conditions. Raman and photoluminescence spectroscopy were employed to assess the optical and electronic quality of MoS₂ grown on h-BN as well as the interactions between MoS₂ and the supporting substrate. Compared to silica, MoS₂ layers grown on h-BN are less prone to oxidation and are subjected to considerably weaker electronic perturbation.

Introduction

Control over the fundamental physical/chemical properties of individual two-dimensional (2D) crystals has reached a satisfactory level, with graphene being the best explored crystal [1]. The next step is to find ways to stack together more than one type of 2D crystals [2, 3] so the improved properties of their assemblage can be exploited. Few attempts have been made so far to prepare "lateral heterostructures"

where two different 2D crystals arrange in a single layer. Lateral heterostructures of graphene and hexagonal boron nitride (h-BN) were investigated due to the small lattice mismatch ($\sim 1.7\%$) enabling the fabrication of heterostructures of randomly distributed domains [4] and shape-controlled lateral heterostructures [5].

The controlled growth of *vertically-stacked* heterostructures of different 2D crystals, or van der Waals heterostructures, also represents an emerging

Address correspondence to E-mail: sny@iceht.forth.gr



¹Foundation for Research and Technology Hellas – Institute of Chemical Engineering Sciences (FORTH/ICE-HT), P.O. Box 1414, 26504 Rio. Patras. Greece

²Department of Materials Science, University of Patras, 26504 Rio, Patras, Greece

³Department of Chemical Engineering, Kansas State University, Manhattan, KS 66506, USA

field of research [6]. As 2D crystals are in principle molecular crystals [7], characterized by strong covalent intra-layer and weak interlayer bonding, stacking different 2D layers on top of each other is a less formidable task than joining laterally different offering opportunities for superlattices with tailored-made structures and Vertical heterostructures properties. combining graphene, h-BN, and various transition metal dichalcogenides (TMDCs) have been demonstrated [8-15]. Mechanical exfoliation has been the main method for their production. While the method provides 2D crystals of high quality, the position of such micron-sized crystals over each other is an inextricable process as it requires several intermediate steps and lacks prospects of scalability. Further, although solvent-based chemical methods have proven useful in preparing large volumes of various 2D crystals, these methods offer limited control in producing heterostructures of desired features. On the other hand, CVD is a viable method for the large-scale, controlled growth of 2D crystals and could thus be used to efficiently grow MoS₂ crystals on pre-deposited h-BN onto a substrate, thus offering cleaner interfaces than the mechanical exfoliation method.

Among TMDCs, MoS₂ is the most systematically explored 2D crystal; it has been studied for several decades, since the pioneering studies by Frindt and collaborators [16, 17], and others [18] with emphasis on the isolation of single layers by mechanical and chemical exfoliation. To date, thin layers of MoS₂ has been produced by several different synthesis routes such as liquid exfoliation [19], chemical vapor deposition on a variety of substrates primarily through the sulfurization of MoO₃ [20], decomposition of precursor compounds [21], sulfurization of Mo thin films pre-deposited on various substrates [22, 23], and direct sulfurization of Mo foils where substrate-scale uniform films with controlled thickness down to one monolayer were prepared by ambient pressure CVD [24]. This vivid interest has arisen mostly from the semiconducting nature of MoS₂ and its direct band gap of ~1.8 eV in the monolayer form. Since the electrical properties of MoS₂ on SiO₂ have been inferior to those of free-standing MoS₂, e.g., unipolar *n*-type behavior and low mobility [25], other substrates such as h-BN have been used. The flatness of the atomically thin inert h-BN layer offers an excellent alternative over silica since—due to its sizeable band gap—MoS₂ is susceptible to undesired traps though the surface dangling bonds of silica [26].

MoS₂/h-BN vertical heterostructures have mostly been prepared by micromechanical exfoliation and transfer [27–31]; only a few attempts have appeared recently of their direct growth using a more scalable method, e.g., CVD [32–36]. Ling et al. [32] presented preliminary data about the growth of MoS₂ on h-BN showing that aromatic molecules used as seeding promoters were indispensable for the growth of large area MoS₂ monolayer growth, whereas, in the absence of seeding, random bulk-like (100 nm in height) MoS₂ particles formed under their growth conditions. Wang et al. [33] employed an all-CVD approach where CVD-grown multilayer h-BN was first transferred onto a Si/SiO₂ substrate. MoS₂ was grown on top of it by reacting MoO₃ and sulfur. Yan et al. [34] used CVD to grow MoS₂ with preferred relative rotation angles on h-BN flakes pre-deposited on Si/SiO2 substrates by exfoliation. Finally, Behura et al. [35] synthesized h-BN directly by oxide-assisted CVD growth and sequentially, without transferring the h-BN film, deposited MoS₂ atop this layer. Wan et al. [36] concluded from experiments and theoretical arguments that the difference in the optical properties between MoS2 grown on h-BN by CVD and SiO₂ originates from a weak doping effect caused by the substrate.

In this article, we present the CVD growth of MoS₂ layers on thick h-BN flakes mechanically exfoliated on Si/SiO₂ substrates. Change of growth conditions reveals novel crystal morphologies as evidenced by electron microcopy. Optical characterization, i.e., Raman and photoluminescence spectroscopy, is used to compare and contrast the electronic and optical properties of MoS₂ layers grown on h-BN and Si/SiO₂.

Experimental details

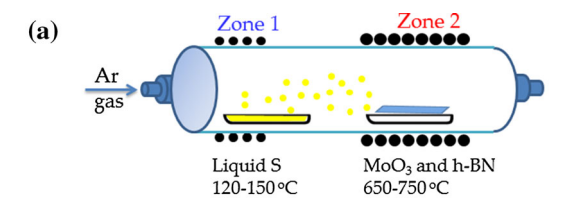
Bulk h-BN crystals were grown by precipitation from a nickel–chromium flux. The crystal growth process was described in detail by Hoffman et al. [37]. Briefly, first hot pressed h-BN was dissolved into the flux by heating to 1550 °C under N₂ atmosphere. Then, h-BN precipitation was induced by slowly cooling (4 °C/h), which reduced its solubility in the flux. After the sample had cooled to room temperature, h-BN flakes were removed by mechanical exfoliation with thermal release tape and transferred to a SiO₂/Si handle



substrate. The thickness of the h-BN flakes was on the order of 20 to 50 microns.

Sulfur (Alfa Aesar 99.999%) and MoO₃ (Alfa Aesar 99.9%) were used for the CVD growth of MoS₂. The substrates with the h-BN flakes were inserted into a three-zone tubular furnace. The CVD chamber was purged with ultrapure Ar at the rate of 100 sscm for 60 min prior to raising the temperature. Sulfur was placed upstream, and its temperature was regulated in the range 130-150 °C. Two sets of experiments were conducted, denoted as A and B in Fig. 1. In experiment A, the Si/SiO₂ substrate with the h-BN flakes was put as a lid on top of the MoO₃ container, thus held practically at the same temperature. In experiment B, the substrate with the h-BN flakes was put downstream at a temperature higher than that of the MoO₃. Table 1 compiles the experimental details for the CVD growth. The flow of Ar at 100 sscm was kept the same for all experiments during the CVD growth and furnace cooling. The furnace was heated to the highest temperature at a rate of 20-30 °C/min, while cooling after the growth took place slowly by switching off the furnace. All experiments took place at ambient pressure.

Electron microscopy images were recorded with a high resolution field-emission scanning electron microscope (FE-SEM) instrument (Zeiss, SUPRA 35VP)



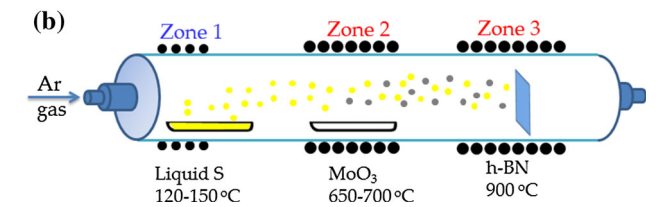


Figure 1 Schematic illustration of the CVD growth experiments **a** top and **b** bottom.

Table 1 Experimental conditions for the CVD growth of MoS₂ on h-BN

# of expt.	T of S (°C)	T of MoO₃ (°C)	T of h-BN (°C)	Duration (min)
A1	150	730	730	5
A2	150	650	650	5
B1	150	700	900	10
B2	150	650	900	10

operating at 15 kV. Raman spectra were accumulated with the 441.6 nm laser line as the excitation source emerging from a He–Cd laser (Kimon). The scattered light was analyzed by the LabRam HR800 (Jobin–Yvon) micro-Raman spectrometer at a spectral resolution of about 2.0 cm $^{-1}$. In addition, PL spectra were excited with the 514.5 cm $^{-1}$ wavelength using the T64000 (Jobin-Yvon) spectrometer. A microscope objective with magnification $50\times$ is used to focus the light onto a spot of \sim 3 μ m in diameter. Low laser intensities were used (\sim 250 μ W on the sample) to avoid spectral changes due to heat-induced effects and to ensure the steady-state photo-excitation density lower than the electron doping by the substrate. The Raman shift was calibrated using Raman band of crystalline Si at 520 cm $^{-1}$.

Results and discussion

Crystal morphology by SEM

Representative FE-SEM images revealing the morphology of MoS₂ crystals grown on h-BN at the conditions of experiment A1 and A2 are shown in Fig. 2. Image (a) displays typical MoS₂ structures grown on h-BN flakes in experiment A1. The inset shows a magnification of the MoS₂ crystals. Their morphology can be described as flat islands surrounding a small but taller protrusion; similar morphologies were reported by Yan et al. [34]. The length of the flat area varied between 100 and 400 nm. The presence of the protrusion possibly signifies the existence of some kind of h-BN lattice defect acting as an energetic nucleation site. Image (b) shows the typical triangularly shaped MoS₂ flakes grown on Si/ SiO₂ substrate, outside the h-BN flake, with an average domain size of $\sim 5 \mu m$. Not all structures are exact triangles, but depending on the presence of nucleation centers (marked by arrows) other irregular shapes also grow. The yield of MoS₂ is higher under the conditions of experiment A2 as is evidenced from Fig. 2c, d. In contrast to the previous case, different morphologies of the grown MoS₂ layers on h-BN are



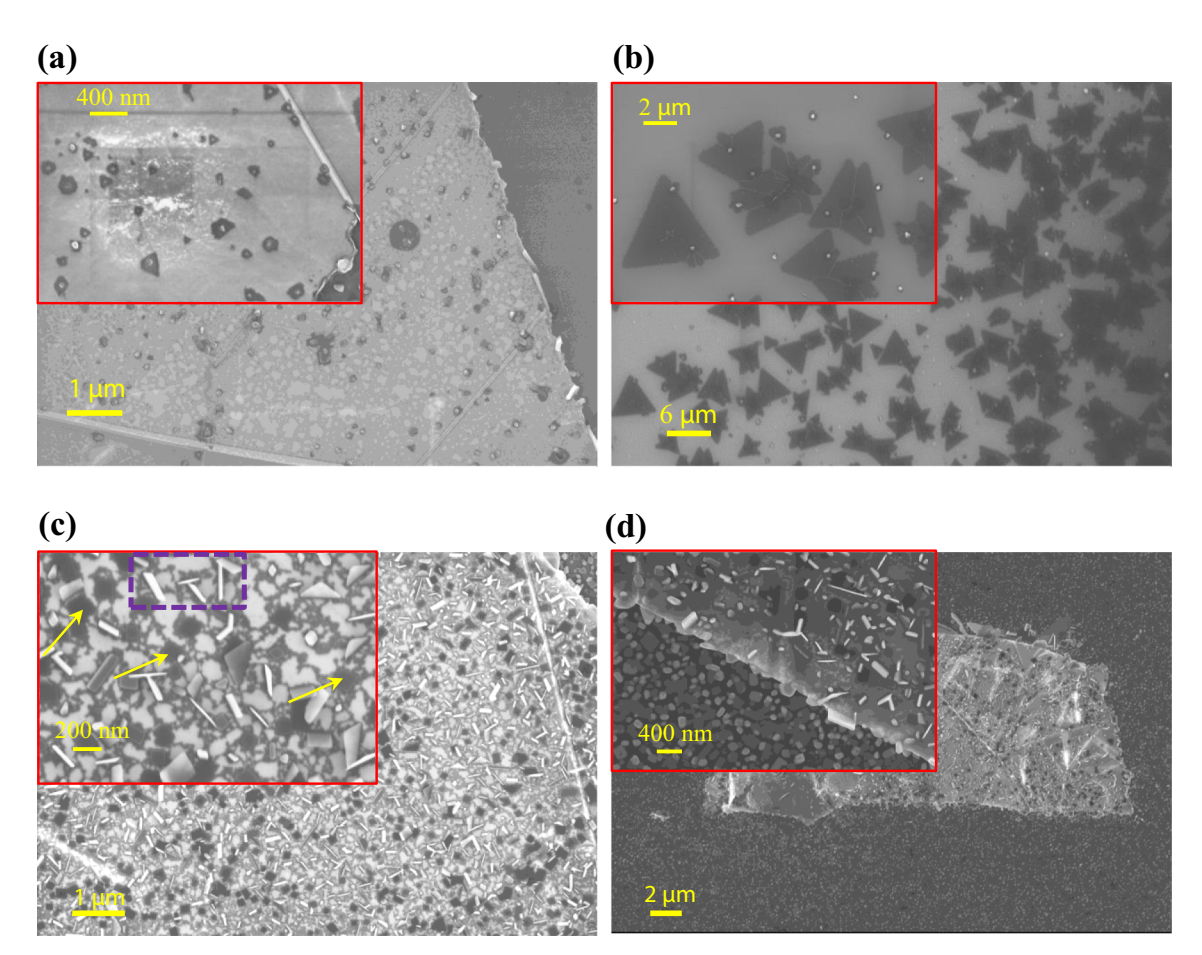


Figure 2 FESEM images of MoS₂ crystals grown on **a** h-BN and **b** Si/SiO₂ under the conditions of experiment A1. Images **c** and **d** illustrate MoS₂ morphology on h-BN in experiment A2. The

rectangular and arrows in the inset of image c denote vertical and in-plane grown MoS₂ crystals, respectively.

observed. Indeed, both planar (in-plane) and vertically grown (normal to the substrate) MoS₂ structures appear on h-BN. Typically, MoS₂ layers on the Si/SiO₂ substrate are dominated by planar morphology, while vertical structures formed on h-BN; details are illustrated in the inset of Fig. 2d. While the growth of vertical isolated coin-like MoS₂ structures is atypical, it has been reported for MoS₂ grown on Mo foils by direct sulfurization of the metal [24]. Similar morphologies were observed for the MoS₂ grown on h-BN under the condition of experiments B1 and B2 as shown in Fig. 3, i.e., both vertical and in-plane structures on h-BN and mainly in-plane structures off h-BN.

Crystal quality and interlayer interactions by Raman scattering

Raman spectroscopy is a fast, reliable, and nondestructive method for evaluating the number of MoS_2 monolayers. Lee et al. [38] established the thickness

dependence of the energy separation of two dominant Raman bands for mechanically exfoliated thin films. The energies of the bands with symmetries E_{2g}^1 and A_{1g} are located at ~ 383 and ~ 408 cm⁻¹, respectively in the bulk crystal. The energy separation of these bands, $\Delta \omega = \omega(A_{1g}) - \omega\left(E_{2g}^1\right)$, is the main indicator used to infer the number of monolayers (nL). Typical values of $\Delta \omega$ for 1L, 2L, 3L, 4L, and bulk are 18.5–19.5, 21.5–22.0, 23.1–23.3, 24.1–24.5, and 25.5 cm⁻¹, respectively [38, 39]. The reliability of this empirical correlation between the number of MoS₂ MLs and the energy difference between the two Raman bands holds not only for layers on SiO₂ but for several others substrates as well, including h-BN [40].

Figure 4(a) shows typical Raman spectra of the MoS_2 layers grown in experiments A1 and A2. Especially, in the case of A2, the frequency difference $\Delta\omega$ follows a uniform and narrow distribution



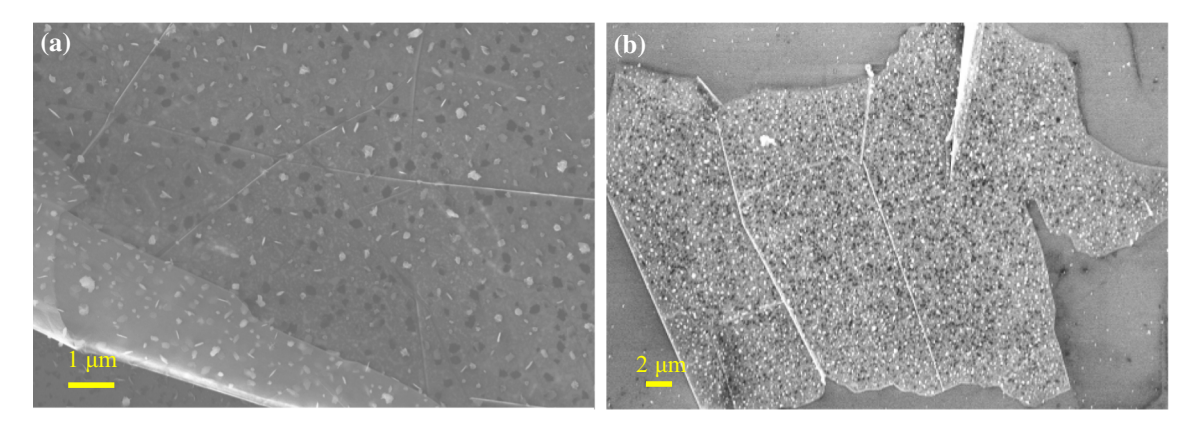


Figure 3 FESEM images of MoS₂ crystals grown on h-BN in experiment B1 (a) and experiment B2 (b).

Table 2 Spectral parameters of the A_{1g} and E_{2g}^1 Raman bands for MoS_2 on h-BN

and

# of expt.	$<\Delta\omega>$ (cm ⁻¹)	FWHM E_{2g}^1 (cm ⁻¹)	FWHM A_{1g} (cm ⁻¹)
A1	22.8 ± 0.9	3.3 ± 0.5	5.2 ± 0.3
A2	22.1 ± 0.7	2.7 ± 0.6	4.4 ± 0.4
B1	24.1 ± 0.2	3.89 ± 0.5	4.96 ± 0.5
B2	23.3 ± 0.9	3.47 ± 0.6	4.67 ± 0.7
1 ML	21.3 ^a ; 23.4 ^b ; 20.6 ^c	5.2 ^a	6.0^{a}
2 ML	22.1 ^a ; 22.7 ^c	5.8 ^a	7.3 ^a

^a From Ref. [30] for MoS₂ exfoliated on h-BN

the interlayer interactions of the heterostructures, across centimeter-scale area. Table 2 compiles various spectral parameters for all samples, extracted by fitting the spectra with Lorentzian lines. The mean values of the difference $<\Delta\omega>=$ $\omega(A_{1g}) - \omega(E_{2g}^1)$ for samples A1 and A2 are 22.8 \pm 0.9 and $22.1 \pm 0.7 \text{ cm}^{-1}$, respectively, which—if interpreted according to the empirical relation [38, 39] of exfoliated MoS₂ on SiO₂—suggests the formation of bilayer and trilayer MoS₂. As we discuss below, the interlayer interactions in heterostructures renormalize the phonon frequencies affecting the energy separation of the A_{1g} and E_{2g}^1 bands, and hence, the empirical correlation between $\Delta\omega$ and the number of MLs has to be considered with care. The mean values of the FWHM for both Raman bands are considerably

indicating consistency in both the MoS₂ layer thick-

Judging from the spectral parameters of these two bands, the growth conditions of experiment A1 and A2 favor the formation of higher quality MoS₂

smaller than the corresponding ones of exfoliated

crystals compared to those of experiment B1 and B2. Notably, judging from the narrower width of the Raman bands, the quality of the CVD-grown MoS₂ is appreciably better than that of the exfoliated MoS₂ deposited on h-BN, in all experiments conducted here [30]. Representative distributions and probabilities of the energy difference $\Delta\omega$, and the FWHM of the E_{2g}^1 and A_{1g} bands for A2 are shown in Fig. 4b–d. Figure 4b makes clear that almost 70% of the measured spectra bear a value for the energy difference $\Delta\omega$ less than ~ 22.5 cm⁻¹, indicating predominant growth of bilayer MoS₂.

The interfaces of atomically thin heterostructures exert measurable effects in their electronic structures, which then affect Raman spectra and PL emission. Such effects were recently explored for single-layer MoS₂ [40]. The frequency difference of the dominant Raman peak $\Delta \omega = \omega(A_{1g}) - \omega(E_{2g}^1)$ was measured as ~ 19.2 and ~ 20.8 cm⁻¹ for exfoliated monolayer MoS_2 on silica and h-BN, respectively. The larger $\Delta\omega$ of MoS₂ on h-BN in relation to $\Delta\omega$ of the free-standing ML arises from the blueshift of the A_{1g} mode,

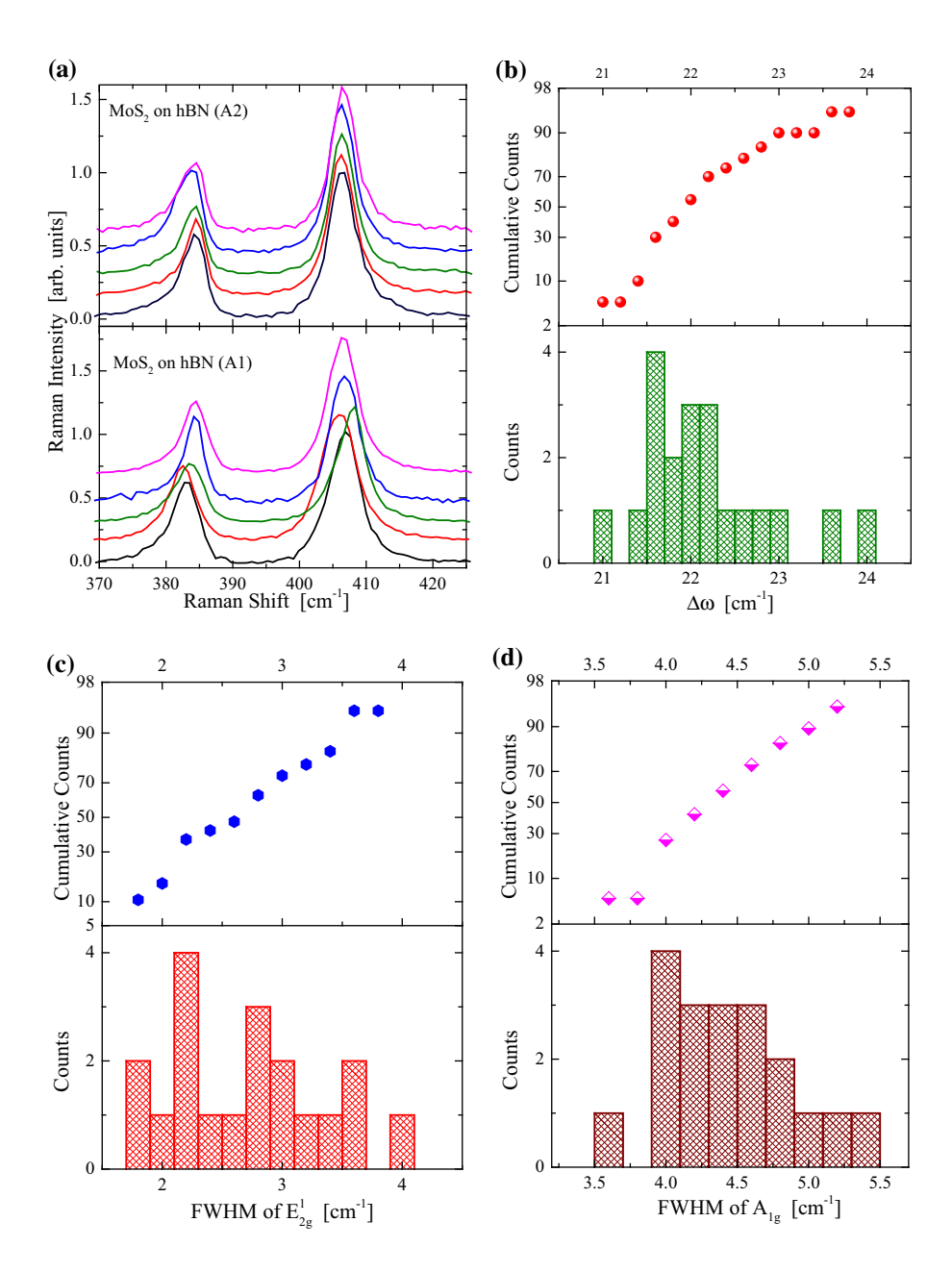


 MoS_2 on h-BN [30].

^b From Ref. [36] for MoS₂ grown on h-BN by CVD

^c From Ref. [40] for MoS₂ exfoliated on h-BN

Figure 4 a Representative Raman spectra of MoS_2 layers grown on h-BN collected across cm-scale areas for sample A1 (bottom) and A2 (top). Distributions and probabilities of the: **b** energy difference $\Delta\omega$, **c** FWHM of the E_{2g}^1 mode and **d** FWHM of the A_{1g} mode.



while the E_{2g}^1 mode does not exhibit appreciable shift for different substrates. The effect was attributed to changes in the doping level as h-BN bears a considerably lower density of charged effects in comparison with silica. The effect on the Raman spectrum of micromechanically exfoliated MoS₂ layers on h-BN was also explored by Li et al. [30], who found larger $\Delta\omega$ differences for BN. They reported that $\Delta\omega$ differs between h-BN and silica substrates by $\sim 3.5~{\rm cm}^{-1}$ for monolayer and $\sim 1~{\rm cm}^{-1}$ for bilayer MoS₂. Both peaks exhibit a blueshift for MoS₂ on h-BN in comparison with their values for the silica substrate. Controlled doping experiments, using exfoliated

monolayer MoS₂ on silica, show that by increasing electron concentration up to 1.8×10^{13} cm⁻², the A_{1g} mode frequency red-shifts by 4 cm⁻¹, while its line width increases by ~ 6 cm⁻¹ [41]. On the contrary, the E_{2g}^1 mode appears much less sensitive to doping. This observation cast doubts on the role of doping as a possible cause of the contrasting behavior of the MoS₂ Raman bands on silica and h-BN substrates. Zhou et al. [42] concluded from similar effects for heterostructures of exfoliated MoS₂ with various 2D crystals that the in-plane mode E_{2g}^1 can be used as an indicator of the in-plane strain, while the out-of-plane mode A_{1g} provides information about the quality of



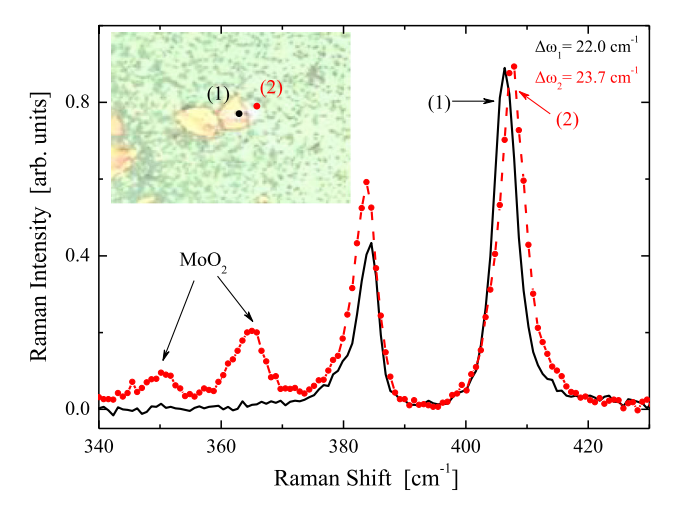


Figure 5 Raman spectra of MoS_2 grown on an h-BN flake (*solid line*) and on the Si/SiO_2 substrate (*solid dots*) in the adjacent area. The spectra are normalized to the intensity maximum of the A_{1g} peak. *Inset* optical micrograph labeling the location of points where Raman spectra were collected.

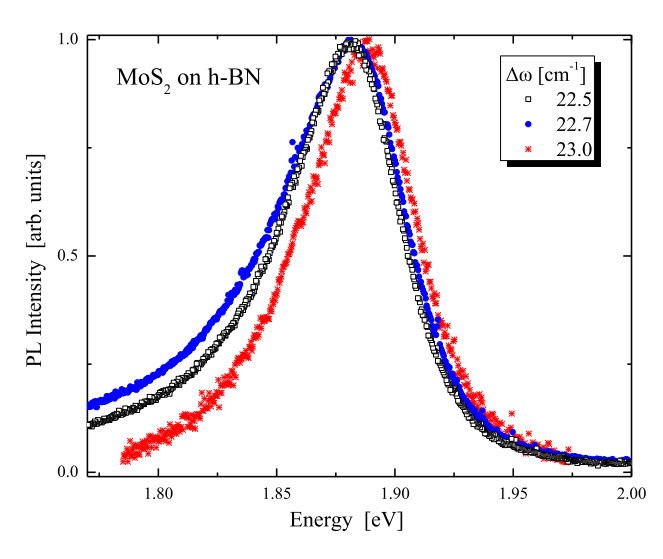


Figure 6 Typical PL spectra of MoS_2 on h-BN for various layers thicknesses.

the interfacial contact. The latter exhibits a blueshift of $\sim 2~\text{cm}^{-1}$ in various exfoliated-prepared heterostructures of MoS₂ with other crystals.

Qualitative differences of MoS₂ grown on h-BN and SiO₂

The preceding discussion revealed the influence of the various substrates on the Raman spectra due to different interactions between the crystal lattices. Here, we point out two qualitative differences between the growth mechanisms of MoS₂ on h-BN and SiO₂.

Analysis of several experiments conducted under exactly the same growth conditions, i.e., in the course of the same experiment, revealed that: (1) MoS₂ films on Si/SiO₂ are, in general, thicker than those gown on h-BN and (2) MoS₂ is less prone to oxidation when grown on h-BN. Figure 5 displays the typical Raman spectra of MoS2 collected from layers grown on a h-BN flake, point (1), and the Si/SiO₂ substrate area located few microns away from the flake, point (2). An optical micrograph is shown in the inset. Raman spectra which correspond to point (1) show bilayer MoS₂ with better crystallinity as dictated by the narrower Raman bands in comparison with those of point (2). On the contrary, Raman spectra of MoS₂ recorded from point (2) reveal thicker MoS₂ layers and partial oxidation of the film as demonstrated by the bands at \sim 350 and \sim 365 cm⁻¹, which are assigned to MoO₂. The higher tendency of MoS₂ toward oxidation at sample areas such as point (2) might arise from the interaction of Mo and the oxygen of the native oxide on Si substrate. The detailed mechanism has been explored by Xu et al. [43]. While not all of the MoS₂ layers grown on Si/SiO₂ are oxidized, all MoS₂ layers on h-BN checked were shown to be free of oxygen. Thus, in the absence of strict oxygen-free conditions, MoS₂ can still grow on h-BN without traces of oxides and with better crystallinity than for MoS₂ grown simultaneously on adjacent SiO₂.

Comparison of photoluminescence emission of CVD-grown MoS₂ on h-BN and SiO₂

The intensity and energy position of the PL band is frequently employed to understand the nature of the MoS₂ interactions with its supporting substrate. The PL profile of MoS₂ reveals two main features: the A band at ~ 1.9 eV (655 nm) and the B band at $\sim 2.0-2.1$ (590-620 nm), representing excitons associated with direct optical transitions. In the presence of charged excitons (trions, i.e., bound state of two electrons to a hole), a new low-energy shoulder A^- at $\sim 1.85 \text{ eV}$ (670 nm) appears near the A exciton [44]. Monolayer exfoliated MoS₂ on h-BN exhibits stronger PL intensity in comparison with MoS₂ on silica. Besides, the energy maximum of the PL band shows a phenomenal blueshift by ca. 10 nm for MoS₂ on h-BN as compared to SiO2, which was accounted for by a relative increase in the luminescence emission from neutral excitons [40]. Alternatively, the extent of the blueshift in the PL band peak indicates that the



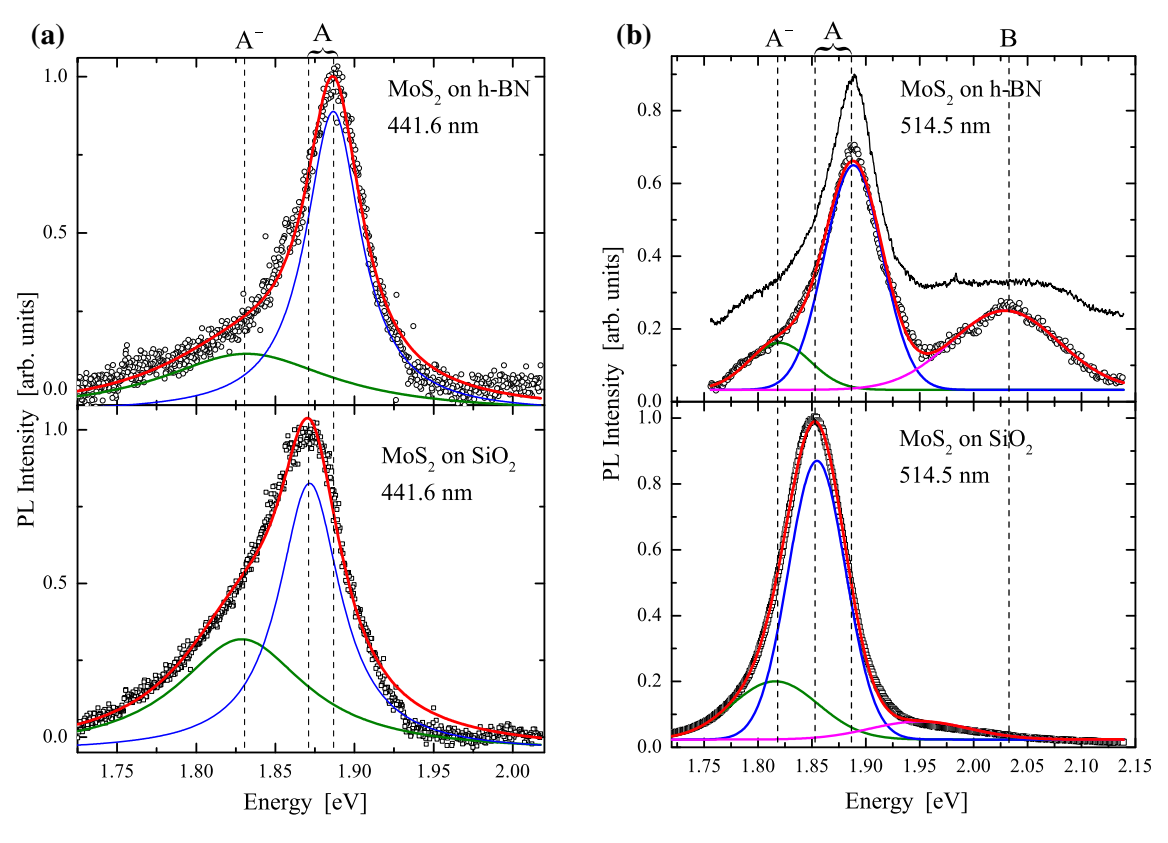


Figure 7 Analysis of PL spectra for MoS₂ grown on SiO₂ and h-BN excited by the a 441.6 nm and the b 514.5 nm laser lines.

substrate affects the relative population of neutral to charged excitons.

PL spectra were recorded from MoS₂ layers grown on both h-BN and Si/SiO₂ using the 441.6 nm excitation laser line showing consistent results in each case. Figure 6 shows representative PL spectra of MoS₂ on h-BN for various layer thicknesses in the range 22.5–23.0 cm⁻¹ revealing minor spectral changes among the various spectra. The B exciton band is absent, or at least very weak, for the case that excitation takes place with the 2.81 eV laser energy (441.6 nm). The A exciton band at \sim 1.88 eV is the dominant feature, while a weak contribution of the A trion is evident by the skewness (low-energy asymmetry) of the PL spectrum. Figure 7 shows a curve fitting analysis of the PL spectra recorded from MoS₂ layers grown on h-BN and Si/SiO₂ using two different excitation energies.

The low relative ratio A^-/A of the PL bands indicates a fairly low density of accumulated charges on MoS_2 from the substrate in both cases, i.e., for silica and h-BN. Notably, the ratio A^-/A is systematically lower for MoS_2 on h-BN compared to that grown on SiO_2 for both excitation wavelengths. As

Mak et al. [44] have shown, the trion A peak intensity is rather insensitive to the doping electron densities while the neutral exciton peak A decreases drastically with increasing the doping density. For the 441.6 nm excitation energy, the intensity ratio A^{-}/A is estimated to be ~ 0.61 and ~ 0.87 for h-BN and SiO₂, respectively, while for the 514.5 nm energy the ratio assumes values of 0.34 and 0.31. As the neutral exciton band A is systematically more intense than the trion A⁻ peak, then based on the work of Sercombe et al. [45] we may expect that the MoS₂ films grown in this work have low electron densities, i.e., less than 10^{12} cm⁻². Indeed, it was shown [45] that mechanically exfoliated MoS2 few-layered films deposited onto silica exhibit large film-to-film variations in their PL spectra. These optical non-uniformities were assigned to strong variations in the local electron charging of MoS₂. Capping MoS₂ with dielectric layers engenders enhancement of negative charging leading to uniform optical properties. On the contrary, CVD-grown MoS2 films grown on h-BN exhibit quite uniform PL patterns. Finally, the position and width of the A peak of MoS₂ grown on h-BN are much closer, compared to that grown on SiO₂, to



the corresponding PL parameters of the free-standing MoS_2 layer [44]. This indicates considerable weaker perturbation of the h-BN substrate to the electronic structure of MoS_2 .

Conclusions

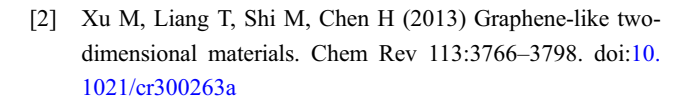
In summary, we have shown that the morphology of MoS₂ on h-BN, which has been pre-deposited on Si/ SiO₂ substrates, can be controlled by adjusting the growth conditions in a CVD experiment in the absence of strict oxygen-free conditions. Planar (in-plane) MoS₂ crystals grow on SiO₂, while planar and atypical vertical (normal to the substrate) MoS₂ structures grow on h-BN. Raman and photoluminescence spectroscopy provided detailed information about the optical and electronic quality of MoS₂ grown on h-BN as well as the interactions between MoS₂ and the supporting substrate. Analyzing the Raman spectra, the spectral parameters A_{1g} and E_{2g}^1 reveals the growth of mostly bilayer MoS₂. The quality of MoS₂ grown in this work is better than that of the exfoliated MoS₂ deposited on h-BN. Further, analysis of several experiments conducted under exactly the same growth conditions revealed that MoS₂ films on Si/SiO₂ are thicker than those gown on h-BN while MoS₂ is less prone to oxidation when grown on h-BN. PL spectra demonstrated that MoS₂ grown on h-BN is subjected to considerably weaker electronic perturbation than that grown on SiO₂. The systematically weaker trion A⁻ peak than the neutral exciton band A casts evidence that MoS2 grown on h-BN under the current conditions exhibit very low electron densities.

Acknowledgements

A. A. and S. N. Y. would like to thank Dr. G. A. Voyiatzis for providing experimental facilities for the Raman spectra. Dr. V. Dracopoulos is thanked for helping with electron microcopy images. The growth of h-BN crystals was supported by the National Science Foundation, CMMI award #1538127.

References

[1] Novoselov KS, Fal'ko VI, Colombo L et al (2012) A road-map for graphene. Nature 490:192–200. doi:10.1038/nature11458



- [3] Butler SZ, Hollen SM, Cao L et al (2013) Progress, challenges, and opportunities in two-dimensional materials beyond graphene. ACS Nano 7:2898–2926. doi:10.1021/nn400280c
- [4] Levendorf MP, Kim C-J, Brown L et al (2012) Graphene and boron nitride lateral heterostructures for atomically thin circuitry. Nature 488:627–632. doi:10.1038/nature11408
- [5] Gong Y, Shi G, Zhang Z et al (2014) Direct chemical conversion of graphene to boron- and nitrogen- and carbon-containing atomic layers. Nat Commun. doi:10.1038/ncomms4193
- [6] Geim AK, Grigorieva IV (2013) Van der Waals heterostructures. Nature 499:419–425. doi:10.1038/ nature12385
- [7] Zallen R, Slade M (1974) Rigid-layer modes in chalcogenide crystals. Phys Rev B 9:1627–1637. doi:10.1103/PhysRevB. 9.1627
- [8] Ponomarenko LA, Geim AK, Zhukov AA et al (2011) Tunable metal-insulator transition in double-layer graphene heterostructures. Nat Phys 7:958–961. doi:10.1038/ nphys2114
- [9] Britnell L, Gorbachev RV, Jalil R et al (2012) Field-effect tunneling transistor based on vertical graphene heterostructures. Science 335:947–950. doi:10.1126/science.1218461
- [10] Haigh SJ, Gholinia A, Jalil R et al (2012) Cross-sectional imaging of individual layers and buried interfaces of graphene-based heterostructures and superlattices. Nat Mater 11:764–767. doi:10.1038/nmat3386
- [11] Georgiou T, Jalil R, Belle BD et al (2012) Vertical field-effect transistor based on graphene–WS2 heterostructures for flexible and transparent electronics. Nat Nanotechnol 8:100–103. doi:10.1038/nnano.2012.224
- [12] Bertolazzi S, Krasnozhon D, Kis A (2013) Nonvolatile memory cells based on MoS₂/graphene heterostructures. ACS Nano 7:3246–3252. doi:10.1021/nn3059136
- [13] Hunt B, Sanchez-Yamagishi JD, Young AF et al (2013) Massive Dirac fermions and Hofstadter butterfly in a van der Waals heterostructure. Science 340:1427–1430. doi:10.1126/ science.1237240
- [14] Yu L, Lee Y-H, Ling X et al (2014) Graphene/MoS₂ hybrid technology for large-scale two-dimensional electronics. Nano Lett 14:3055–3063. doi:10.1021/nl404795z
- [15] Zhang W, Chuu C-P, Huang J-K et al (2014) Ultrahigh-gain photodetectors based on atomically thin graphene–MoS₂ heterostructures. Sci Rep. doi:10.1038/srep03826
- [16] Frindt RF (1966) Single crystals of MoS₂ several molecular layers thick. J Appl Phys 37:1928. doi:10.1063/1.1708627



- [17] Yang D, Sandoval SJ, Divigalpitiya WMR et al (1991) Structure of single-molecular-layer MoS₂. Phys Rev B 43:12053–12056. doi:10.1103/PhysRevB.43.12053
- [18] Schumacher A, Scandella L, Kruse N, Prins R (1993) Single-layer MoS₂ on mica: studies by means of scanning force microscopy. Surf Sci Lett 289:L595–L598. doi:10.1016/0167-2584(93)90727-Z
- [19] Eda G, Yamaguchi H, Voiry D et al (2011) Photoluminescence from chemically exfoliated MoS₂. Nano Lett 11:5111–5116. doi:10.1021/nl201874w
- [20] Lee Y-H, Zhang X-Q, Zhang W et al (2012) Synthesis of large-area MoS₂ atomic layers with chemical vapor deposition. Adv Mater 24:2320–2325. doi:10.1002/adma.201104 798
- [21] Liu K-K, Zhang W, Lee Y-H et al (2012) Growth of largearea and highly crystalline MoS₂ thin layers on insulating substrates. Nano Lett 12:1538–1544. doi:10.1021/nl2043612
- [22] Jäger-Waldau A, Lux-Steiner MC, Bucher E et al (1993) MoS₂ thin films prepared by sulphurization. Appl Surf Sci 65–66:465–472. doi:10.1016/0169-4332(93)90703-E
- [23] Zhan Y, Liu Z, Najmaei S et al (2012) large-area vapor-phase growth and characterization of MoS₂ atomic layers on a SiO2 substrate. Small 8:966–971. doi:10.1002/smll.20110 2654
- [24] Antonelou A, Syrrokostas G, Sygellou L et al (2016) Facile, substrate-scale growth of mono- and few-layer homogeneous MoS₂ films on Mo foils with enhanced catalytic activity as counter electrodes in DSSCs. Nanotechnology 27:45404. doi:10.1088/0957-4484/27/4/045404
- [25] Bao W, Cai X, Kim D et al (2013) High mobility ambipolar MoS₂ field-effect transistors: substrate and dielectric effects. Appl Phys Lett 102:42104. doi:10.1063/1.4789365
- [26] Radisavljevic B, Radenovic A, Brivio J et al (2011) Singlelayer MoS₂ transistors. Nat Nanotechnol 6:147–150. doi:10. 1038/nnano.2010.279
- [27] Chan MY, Komatsu K, Li S-L et al (2013) Suppression of thermally activated carrier transport in atomically thin MoS₂ on crystalline hexagonal boron nitride substrates. Nanoscale 5:9572. doi:10.1039/c3nr03220e
- [28] Lee G-H, Yu Y-J, Cui X et al (2013) Flexible and transparent MoS₂ field-effect transistors on hexagonal boron nitride– graphene heterostructures. ACS Nano 7:7931–7936. doi:10. 1021/nn402954e
- [29] Cui X, Lee G-H, Kim YD et al (2015) Multi-terminal transport measurements of MoS₂ using a van der Waals heterostructure device platform. Nat Nanotechnol 10:534–540. doi:10.1038/nnano.2015.70
- [30] Li L, Lee I, Lim D et al (2015) Raman shift and electrical properties of MoS₂ bilayer on boron nitride substrate.

- Nanotechnology 26:295702. doi:10.1088/0957-4484/26/29/295702
- [31] Lee G-H, Cui X, Kim YD et al (2015) highly stable, dual-gated MoS₂ transistors encapsulated by hexagonal boron nitride with gate-controllable contact, resistance, and threshold voltage. ACS Nano 9:7019–7026. doi:10.1021/acsnano.5b01341
- [32] Ling X, Lee Y-H, Lin Y et al (2014) Role of the seeding promoter in MoS₂ growth by chemical vapor deposition. Nano Lett 14:464–472. doi:10.1021/nl4033704
- [33] Wang S, Wang X, Warner JH (2015) All chemical vapor deposition growth of MoS₂: h-BN vertical van der Waals heterostructures. ACS Nano 9:5246–5254. doi:10.1021/acs nano.5b00655
- [34] Yan A, Velasco J, Kahn S et al (2015) Direct growth of single- and few-layer MoS₂ on h-BN with preferred relative rotation angles. Nano Lett 15:6324–6331. doi:10.1021/acs. nanolett.5b01311
- [35] Behura S, Nguyen P, Che S et al (2015) Large-area, transfer-free, oxide-assisted synthesis of hexagonal boron nitride films and their heterostructures with MoS₂ and WS2. J Am Chem Soc 137:13060–13065. doi:10.1021/jacs.5b07739
- [36] Nozaki J, Kobayashi Y, Miyata Y et al (2016) Local optical absorption spectra of h-BN-MoS₂ van der Waals heterostructure revealed by scanning near-field optical microscopy. Jpn J Appl Phys 55:06GB01. doi:10.7567/JJAP. 55.06GB01
- [37] Hoffman TB, Clubine B, Zhang Y et al (2014) Optimization of Ni-Cr flux growth for hexagonal boron nitride single crystals. J Cryst Growth 393:114-118. doi:10.1016/j.jcrys gro.2013.09.030
- [38] Lee C, Yan H, Brus LE et al (2010) Anomalous lattice vibrations of single- and few-layer MoS₂. ACS Nano 4:2695–2700. doi:10.1021/nn1003937
- [39] Li H, Zhang Q, Yap CCR et al (2012) From bulk to monolayer MoS₂: evolution of Raman scattering. Adv Funct Mater 22:1385–1390. doi:10.1002/adfm.201102111
- [40] Buscema M, Steele GA, van der Zant HSJ, Castellanos-Gomez A (2014) The effect of the substrate on the Raman and photoluminescence emission of single-layer MoS₂. Nano Res 7:561–571. doi:10.1007/s12274-014-0424-0
- [41] Chakraborty B, Bera A, Muthu DVS et al (2012) Symmetry-dependent phonon renormalization in monolayer MoS₂ transistor. Phys Rev B 85:161403. doi:10.1103/PhysRevB. 85.161403
- [42] Zhou K-G, Withers F, Cao Y et al (2014) Raman modes of MoS₂ used as fingerprint of van der Waals interactions in 2-D crystal-based heterostructures. ACS Nano 8:9914–9924. doi:10.1021/nn5042703



- [43] Xu X, Goodman DW (1993) The preparation and characterization of ultra-thin silicon dioxide films on a Mo(110) surface. Surf Sci 282:323–332. doi:10.1016/0039-6028(93) 90937-F
- [44] Mak KF, He K, Lee C et al (2012) Tightly bound trions in monolayer MoS₂. Nat Mater 12:207–211. doi:10.1038/nmat3505
- [45] Sercombe D, Schwarz S, Del Pozo-Zamudio O et al (2013) Optical investigation of the natural electron doping in thin MoS_2 films deposited on dielectric substrates. Sci Rep. doi:10.1038/srep03489

